 doi:10.20944/preprints202209.0421.v1

Article

High piezoelectric output voltage from blue fluorescent *N,N*-dimethyl-4-nitroaniline nano crystals into poly-l-lactic acid electrospun fibers

Rosa M.F. Baptista [1,*] Bruna Silva [1], João Oliveira [1], Vahideh B. Isfahani [1], Bernardo Almeida [1], Mário R. Pereira [1], Nuno Cerca [2], Cidália Castro [3], Pedro V. Rodrigues [3], Ana Machado [3], Michael Belsley [1] and Etelvina de Matos Gomes [1]

[1] Centre of Physics of Minho and Porto Universities (CF-UM-UP), University of Minho, Campus de Gualtar, 4710-057 Braga, Portugal
[2] Centre of Biological Engineering, University of Minho, Campus Gualtar, 4710-057 Braga, Portugal
[3] Institute for Polymers and Composites, University of Minho, Campus de Azurém, 4800-058 Guimarães
* Correspondence: rosa_batista@fisica.uminho.pt

Abstract: *N,N*-dimethyl-4-nitroaniline (NNDM4NA, $C_8H_{10}O_2N_2$), is a superelastic and superplastic charge-transfer molecular crystal with a high molecular dipole moment, μ=7.95 D, which crystallizes in the acentric polar point group 2. Highly aligned poly-l-lactic acid (PLLA) polymer microfibers with embedded NNDM4NA nanocrystals were fabricated using the electrospinning technique. The composite fibers display an extraordinarily high piezoelectric output response, where for a small stress of 5.0×10^3 Nm^{-2}, an effective piezoelectric voltage coefficient of g_{eff}=3.6 VmN^{-1} was obtained. The fibers were found to display solid state blue fluorescence with a long (147 ns) lifetime decay. Furthermore, the composite fibers exhibit an average increase of 67% on the Young modulus reaching 55 MPa, while the tensile strength reaches 2.8 MPa when compared with solely PLLA fibers. The results show that nanocrystals, from small organic molecules, with elastic and piezoelectric properties form hybrid functional 2-dimensional luminescent array which are mechanical strong and generate high output voltages making them promising for applications in energy harvesting and as solid-state blue emitters.

Keywords: Electrospinning, microfibers, piezoelectric crystals, composites, nitroanilines, fluorescence, functional organic materials

1. Introduction

Organic acentric crystals are excellent candidates for applications as piezoelectric, nonlinear and electro-optical materials. Those containing nitroaniline derivative molecules are the simplest ones displaying the highest piezoelectric and nonlinear optical properties. The push–pull conjugated charge-transfer, D^+-π-A^-, molecular systems formed by intramolecular electron donor (D)-acceptor (A) groups are able to form supramolecular assemblies due to molecular dipole-dipole interactions, mediated by hydrogen bonds and other non-covalent interactions. These molecules have very high polarizabilities and hyperpolarizabilities and are among the best candidates for a wide range of piezoelectric and photonic applications [1-4].

The archetype charge-transfer (CT) nitroaniline isomeric molecules are para-nitroaniline or 4-nitroaniline (4NA or pNA, $C_6H_6N_2O_2$) and meta-nitroaniline or 3-nitroanilie (3NA or mNA, $C_6H_6N_2O_2$) with dipole moments of μ=8.2 D and μ=6.9 D, respectively [5]. While pNA crystallizes in the centrosymmetric point group 2/*m* [6], due to a molecular pairwise antiparallel alignment in the crystal unit cell, mNA crystallizes in the acentric point group mm2. Piezoelectricity is therefore forbidden by symmetry in pNA while mNA has one of the largest bulk piezoelectric coefficients measured on a molecular

Preprints (www.preprints.org) | NOT PEER-REVIEWED | Posted: 27 September 2022 doi:10.20944/preprints202209.0421.v1

crystal, d_{31} = 31×10^{-12} NC^{-1}. It is also a strong electro-optic and nonlinear optical organic crystal [7-8].

Adding to the molecules π-electron-donating groups such as OCH_3, NH_2 and $N(CH_3)_2$ leads to an increased asymmetric charge distribution resulting in higher dipole moments, polarizability and hyperpolarizability [9]. An example is 2-methyl-4-nitroaniline (MNA, $C_7H_8N_2O_2$) with a large molecular dipole moment equal to μ=8.1 D and hyperpolarizability β = 71×10^{-40} m^{4}V^{-1} at the wavelength of maximum absorption of 361 nm. It crystallizes in the acentric point group m and displays in the solid state a crystal dipole moment of μ = 19.5 D [10] originating a large piezoelectric coefficient, d_{31} = 13.8×10^{-12} NC^{-1} [11]. MNA is a prototype nonlinear optical and electro-optic crystal [12-14].

Another engineered pNA derivative molecule, although much less attention has been given to it, is *N*,*N*-dimethyl-4-nitroaniline (NNDM4NA, $C_8H_{10}O_2N_2$) with each hydrogen atom on the NH_2 group substituted by a CH_3 group, having the dimethyl and nitro groups at the *para* position on the benzene ring, which crystallizes in the polar point group 2 (Space group $P2_1$) [15]. The molecule has also a high molecular dipole moment, μ= 7.95 D, similar to MNA [16]. Very importantly, NNDM4NA was recently discovered to exhibit superplastic and superelastic properties through slip and twinning deformations dependent on the applied force direction: at room temperature superplasticity occurs when strain is applied along <100> and is accompanied by superelastic behaviour along <201>, keeping single crystallinity during deformation [17]. Superplasticity, the ability to exhibit exceptionally large elongations during tensile deformation, is a well-known property displayed by metals, alloys and polymers [18-19]. However, those are rare property of organic crystals which is presently an important research area, as plastic and flexible organic crystals are of most importance for applications as mechanical actuators, bioelectronics and photonics [20-23].

Electrospinning is an effective nanofabrication technique where an electro hydrodynamic thrust is created by an intense electrostatic field allowing the production of continuous micro/nanofibers from extrusion of a charged polymer fluid. The polymer fibers have high surface-to-volume ratio, light weight and an interconnected porous structure. The technique experimental accessibility and versatility has enabled the preparation of nanomaterials from a remarkably broad class of macromolecular-based systems [24-26]. The functional properties of electrospun fibers are therefore determined by the chemical nature of electrospinning materials solutions, the different processing conditions as well the polymer crystallinity and its molecular orientation inside the micro/nanofibers [27-28]. The technique has been used as a method for producing aligned polymer doped micro/nanofibers with a high degree of guest molecular polar orientation within the polymer. A large variety of organic molecules, from small nitroaniline derivatives to supramolecular dipeptides molecules, with enhanced piezoelectric and nonlinear optical second harmonic generation have been embedded into electrospun fibers [27, 29-36].

Studies of 3NA nanocrystals embedded in poly-ε-caprolactone (PCL) polymer nanofibers showed both enhanced SHG response and piezoelectric output voltage as a mechanical to electrical energy converter, with an instantaneous density power of 122 nWcm^{-2} magnitude similar to that displayed by poly(vinylidene fluoride) and poly(γ-methyl L-glutamate) composite fibers [33].

PLLA is a chiral biodegradable and biocompatible polymer containing two 10/3 helical chains along c crystallographic axis of an orthorhombic base centered unit cell and a huge optical rotatory power (9000 ° mm^{-1}) [37]. Oriented films of PLLA show a piezoelectric bulk shear coefficient d_{14} = 10 pCN^{-1} [38].

In this work NNDM4NA nanocrystals were embedded into aligned PLLA microfibers (NNDM4NA@PLLA), fabricated using the electrospinning technique, forming a hybrid functional material. We report its extraordinary high piezoelectric output response, where for an applied periodical force of 1.5 N (stress 5.0x10^3 Nm^{-2}), an effective piezoelectric voltage coefficient of g_{eff} = 3.6 VmN^{-1} is obtained, five times higher than that from two-dimensional hybrid ferroelectric perovskite of (4-

 doi:10.20944/preprints202209.0421.v1

aminotetrahydropyran)2 lead tetrabromide $(ATHP)_2PbBr_4$) which exhibited an already large value of g_{eff} = 0.66 VmN^{-1}. That very high value resulted from of the superplastic properties of NNDM4NA nanocrystals together with the piezoelectric properties of PLLA polymer. Furthermore, NNDM4NA both in solution and when embedded into electrospun PLLA fibers, NNDM4NA@PLLA, display strong blue fluorescence with a 147 ns long lifetime decay.

2. Materials and Methods

2.1. Solution preparation

NNDM4NA was purchased from Sigma-Aldrich and used as received. Poly (L-lactic acid) (PLLA, Mw 217-225000), was purchased from Polysciences. All solvents were purchased from Sigma-Aldrich and used as received. The precursor electrospinning solution was prepared by dissolving in 4 mL of dichloromethane (DCM) 0.5 g of PLLA with vigorous stirring (700 rpm) at 40 ºC during 1 h (IKA RCT basic, Germany). After complete dissolution, 0,17 g of NNDM4NA previously dissolved in 1 mL of dimethylformamide (DMF) was added to the polymer solution. The resulting solution with a concentration of 10 wt % was stirred for several hours under ambient conditions, prior to the electrospinning process.

2.2. Electrospinning of microfibers

NNDM4NA@PLLA composite microfibers (1:3) were electrospun using a conventional electrospinning apparatus described before in detail [29]. The previously prepared clear and homogenous solution, was loaded into a plastic syringe with a blunt-ended needle with 0.5 mm inner diameter. The syringe was located on a syringe pump and connected to the anode of a high voltage power supply (Spellman CZE2000). Electrospinning was performed at room temperature and various parameters were adjusted to obtain bead free fibers and stable spinning conditions, namely, the solution feeding flow rate, the electric potential difference and the needle tip-collector distance. An electric potential difference of 18 kV was established between the syringe needle and a grounded rotatory collector. The needle-collector distance was 12 cm and flow rate 0.19 mL/h. The aligned fibers were collected on a rotatory mandrel rotating at rate of 300 rpm coated with high purity aluminium foil. Fibers collected on a rapidly rotating mandrel oriented themselves along the mandrel rotating direction due to mechanical stretching forces inherent to the fabrication process.

2.3. Characterization techniques

Crystallinity and crystallographic orientation of *N,N*-dimethyl-4-nitroaniline were studied by X-ray diffraction. The diffraction pattern using θ–2θ scans was recorded between 5º and 40º on a Philips PW-1710 X-Ray diffractometer with Cu-K_α radiation of wavelength 1.5406 Å. The lattice planes parallel to the substrate surface were determined from the reciprocal lattice vector of modulus $(2/\lambda)\sin\theta$, with λ the radiation wavelength and θ the diffraction Bragg angle. Morphology, distribution of diameters and thickness of fibers were accessed through a Scanning Electron Microscope Nova NanoSEM operated at an accelerating voltage of 10 kV. NNDM4NA@PLLA nanofibers were deposited on a silica surface and previously covered with a thin film (10 nm thickness) of Au-Pd (80-20 weight %) using a high-resolution sputter cover, 208HR Cressington Company, coupled to a MTM-20 Cressigton high resolution thickness controller. The diameter range of the produced nanofibers was measured through SEM images using image-analysis software ImageJ 1.51n (NIH, https://imagej.nih.gov/ij/). Average diameter and diameter distribution were determined by measuring 79 random nanofibers from the SEM images and fiber diameter distributions fit to a log-normal function. Fiber array thickness was measured using a Mitutoyo IP 65 micrometer.

 doi:10.20944/preprints202209.0421.v1

Elastic modulus, stress at yield (at 0.2% offset), tensile strength and strain at break (at 60% of tensile strength) were measured using an universal tensile testing machine Zwick / Roell Z005, following the ASTM D882-02 standard. Several 10 x 30 mm specimens, with a gauge length of 16 mm, were tested alongside the oriented fiber direction under a cross-head velocity of 25 mm/min.

Optical absorption (OA) spectra were measured on a Shimadzu UV/2501PC spectrophotometer (Duisburg, Germany) in the wavelength range of 250–480 nm. The Photoluminescence (PL) spectrum, measured at the maximum absorption wavelength as excitation wavelength, was collected using a FluoroMax-4 spectrophotometer (Horiba Jovin Yvon, Madrid, Spain) in the wavelength range of 400–750 nm at room temperature. For these measurements a 10^{-4} M ethanol solution of NNDM4NA was prepared and put in quartz cuvettes with 10^{-2} m path length. Input and output slits were fixed at 5 nm. The fibers luminescence was also observed with an Olympus™ FluoView FV1000 (Olympus, Tokyo, Japan) confocal scanning laser microscope, using a 40x objective and excitation wavelength of 405 nm.

The dielectric properties were characterized by impedance spectroscopy, at temperatures from 15º C to 100º C and in the frequency range 10Hz-3MHz. In order to perform the measurements, the nanofiber array samples were connected forming a parallel plate capacitor included in a LCR network. The electrical contacts on the mats top and bottom surfaces had 10 mm in diameter and were made with air cured silver paste. The complex permittivity $\varepsilon = \varepsilon' - i\varepsilon''$, with ε' and ε'' the real and imaginary parts, respectively calculated from the measured capacitance, $C = \varepsilon' \varepsilon_0 (A/d)$ and loss tan $\delta = \varepsilon''/\varepsilon'$ with A the electrodes contact area, ε_0 the vacuum permittivity and d the array thickness. A Waine Kerr 6440A Precision Component Analyzer connected to a dedicated computer and software, were used in to acquire the data [40]. Shielded test leads were employed to avoid parasitic impedances due to the connecting cables. The temperature dependent measurements were performed with a rate ramp of 2º C/min, using a Polymer Labs PL706 PID controller and furnace.

Piezoelectric output voltage and current were measured across a 100 MΩ load resistance connected to a low pass filter followed by a low noise pre-amplifier (Research systems SR560) before being registered by a Digital Storage Oscilloscope (Agilent Technologies DS0-X-3012A). The fiber array sample with 20x20 mm^2 area (600 μm thickness) was submitted to applied periodic mechanical forces imposed by a vibration generator (Frederiksen SF2185) with frequency of 3 Hz determined by a signal generator (Hewlett Packard 33120A). The forces applied were previously calibrated using a force sensing resistor (FSR402, Interlink Electronics Sensor Technology). The fibers were directly deposited, during the electrospinning process, on high purity aluminium foil, which served as electrodes. The samples were fixed on a stage and forces were applied uniformly and perpendicularly over the surface area of each sample. A schematic set-up is shown in Figure 5 c).

3. Results and Discussion

3.1. Fiber morphology and crystallinity

The microfibers are yellow colored under day light and form a two-dimensional array of highly aligned fibers with 1.38 μm average diameter, Figures 1 a) and b). The surface of each fiber is smooth, Figure 1 c), with no beads or crystals grown on it, having all the NNDM4NA crystals in the fiber interior and evenly spread inside the fibers, as confocal microscopy images show in Figure 2b). These mutually aligned fibers are the result of both the electrospinning processing parameters chosen combined with the mechanical stretching forces present during collection on a rotatory drum, as reported before for MNA_PLLA fibers [29].

Preprints (www.preprints.org) | NOT PEER-REVIEWED | Posted: 27 September 2022 doi:10.20944/preprints202209.0421.v1

The FTIR-ATR spectra collected (Supplementary information, SI, Figure S1), confirms the incorporation of NNDM4NA molecules inside the polymer matrix, as the main bands observed for a polycrystalline sample are also observed for the electrospun fibers.

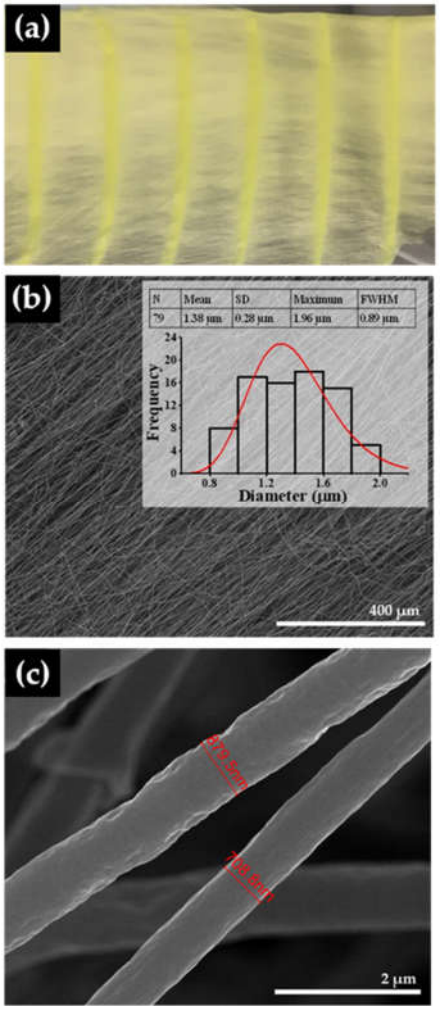

Figure 1. (a) Electrospun NNDM4NA@PLLA nanofiber array as collected on a rotatory drum; SEM images and diameter distributions with average fiber diameters (Mean), standard deviation (SD) and full width at half maximum (FWHM) at 250x **(b)** and 50,000x **(c)** magnification level. The fiber diameter distribution was fit to a log-normal function.

The X-ray diffraction pattern measure, Figure S2, shows that NNDM4NA is crystallized inside the polymer matrix with random orientation. The observed Bragg reflections have been assigned from the known crystal structure. The crystallite size calculated using the Debye-Scherrer equation (SI, Table S1) indicated an average size of 38 nm.

3.2. Optical absorption and luminescence

An NNDM4NA ethanol solution presents an intense absorption band in the range of 300-450 nm, with maximum at 386 nm wavelength arising from CT π-π* transitions [41-42]. Excitation at the maximum absorption wavelength originates in the PL spectrum an intense emission band with maximum at 460 nm, in the blue region, with a full width at

Preprints (www.preprints.org) | NOT PEER-REVIEWED | Posted: 27 September 2022 doi:10.20944/preprints202209.0421.v1

half-maximum of 67 nm (see Figure 2) and a Stokes shift of 74 nm. The PL spectrum of a NNDM4NA@PLLA fiber array shows a maximum emission wavelength at 510 nm, with a full width at half-maximum of 70 nm, exhibiting a red shift of 124 nm (an additional of 50 nm relatively to that in solution), Table 1. This high bathochromic shift towards the long wavelength of CT transition indicates a more extended conjugation, which may be attributed to the stretched molecular conformations along the fiber longitudinal axis as a result of the stretching of polymer fibers, due to extensional flow, during the electrospinning process. FTIR results are in accord to these conclusions as shifts from some bands were observed for the fiber array.

The emission from a nanofiber array was further studied by fluorescence confocal microscopy with excitation at 405 nm. The embedded NNDM4NA nanocrystals displayed a bright blue light revealing emission uniformity along the fibers, Figure 2 b). The strong blue emission from NNDM4NA@PLLA fibers must have been favored by the fibers alignment and stretching imposed by the rotatory drum collector during the electrospinning process. It has been reported that the collection of electrospun nanofibers on a rotatory drum originates both aligned as well stretched fibers with increased photoluminescence [43], which together with a more effective molecular packing at nanoscale contributes to the Stokes shift of the observed emission [32]. Emission at blue wavelengths is of great importance for applications in luminescent devices [44], as only a few compounds have a significant increase in their light emission in their solid state overcoming the problem of aggregation quenching. Importantly, NNDM4NA nanocrystals embedded into PLLA electrospun fibers is therefore one of them.

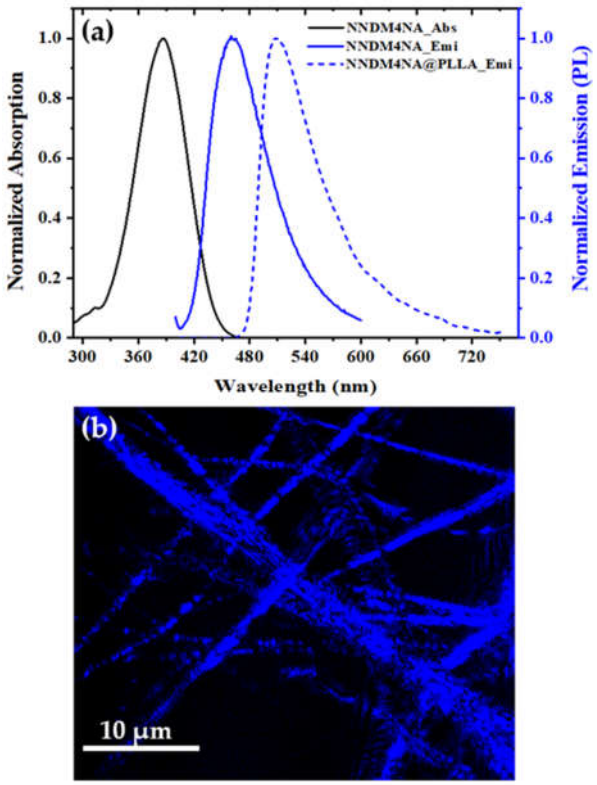

Figure 2. (a) Normalized optical absorption (full black line) and photoluminescence spectra (full blue line) of NNDM4NA in an ethanol at 10^{-4} M concentration; Normalized PL spectrum (dashed blue line) from an NNDM4NA@PLLA fiber mat. PL spectra were measured using the maximum absorption wavelength as the excitation wavelength, λ_{exc}=386 nm; **(b)** Confocal microscopy fluorescence image (50 X 50 µm) of NNDM4NA@PLLA fibers. The fluorescence was observed in the wavelength range of 430–470 nm following excitation at a wavelength λ_{exc} = 405 nm.

 doi:10.20944/preprints202209.0421.v1

Table 1. Absorption and emission data for NNDM4NA in an ethanol solution at 1.0E-4 M concentration, and embedded into polymer fibers.

Sample	λ_{abs} [nm]	λ_{aexc} [nm]	λ_{emi} [nm]	Stokes Shift [nm]
NNDM4NA	386	386	460	74
NNDM4NA@PLLA	—	386	510	124

Fluoresce lifetime decay studied in detail, using a Single Photon Counting equipment, showed that there is a main component of fluorescence, (Figure S4) of NNDM4NA@PLLA fiber array, which accounts for 92% of the all fluorescence emitted having a lifetime decay of 147 ns. The fluorescence has also small contribution (8% total) from two other components both with very short decay times (less than 5 ns) as indicated in Table S2.

3.3. Mechanical Performance

The results from tensile characterization are shown in Figure 3. NNDM4NA@PLLA fibers exhibit good mechanical performance: there is an average increase of 67% on the Young modulus reaching 55 MPa, while the tensile strength reaches 2.8 MPa when compared with PLLA fibers. Both stress at yield and tensile strength have a positive variation of 50%. This significant increase of tensile strength and Young modulus of doped electrospun fibers indicates that hybrid NNDM4NA@PLLA array are stiffer and mechanically stronger than neat PLLA fibers. This increase must be related with the superelastic properties reported for NNDM4NA crystals, where for a small tensile strain (inferior to 100%) there is an increase of the tensile stress [17]. There is a decrease of 53% of the strain at break for doped fibers indicating a decrease in their plasticity. This may be explained from the presence of NNDM4NA nanocrystals inside the polymer matrix which act as a discontinuous phase inhibiting the capability of PLLA chains to flow between themselves thus limiting the creep of molecular chains accompanied by an increase of the polymer chain rigidity [46].

Preprints (www.preprints.org) | NOT PEER-REVIEWED | Posted: 27 September 2022 doi:10.20944/preprints202209.0421.v1

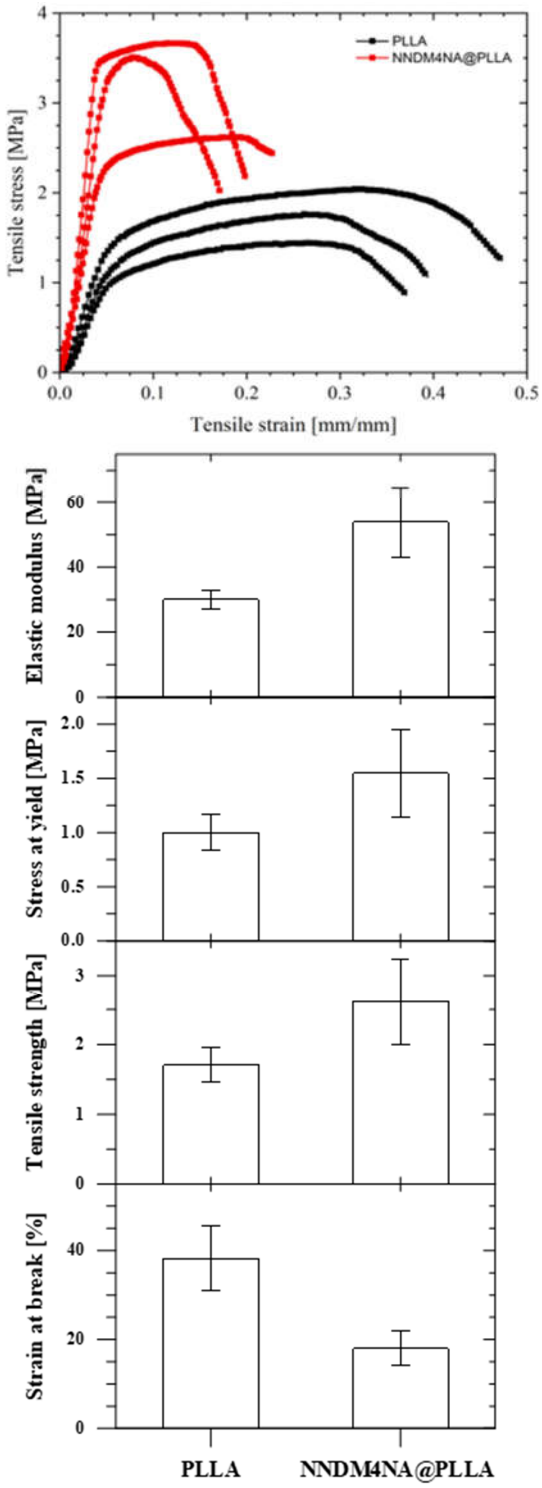

Figure 3. Elastic modulus, stress at yield, tensile strength and strain at break of PLLA and NNDM4NA@PLLA electrospun fibers.

3.4. Dielectric permittivity

Figure 4 a) shows temperature dependence of the real part of the dielectric permittivity (ε′) for composite, NNDM4NA@PLLA fibers, and correspondent measurements in pure PLLA nanofibers. Both curves follow similar trends: until 45 ºC

Preprints (www.preprints.org) | NOT PEER-REVIEWED | Posted: 27 September 2022 doi:10.20944/preprints202209.0421.v1

there is no variation of the dielectric constant with temperature, rising afterwards steeply with two step like anomalies one at ~ 55 ºC and other at ~ 65 ºC correspondent to PLLA fibers glass transition temperature [47-48].

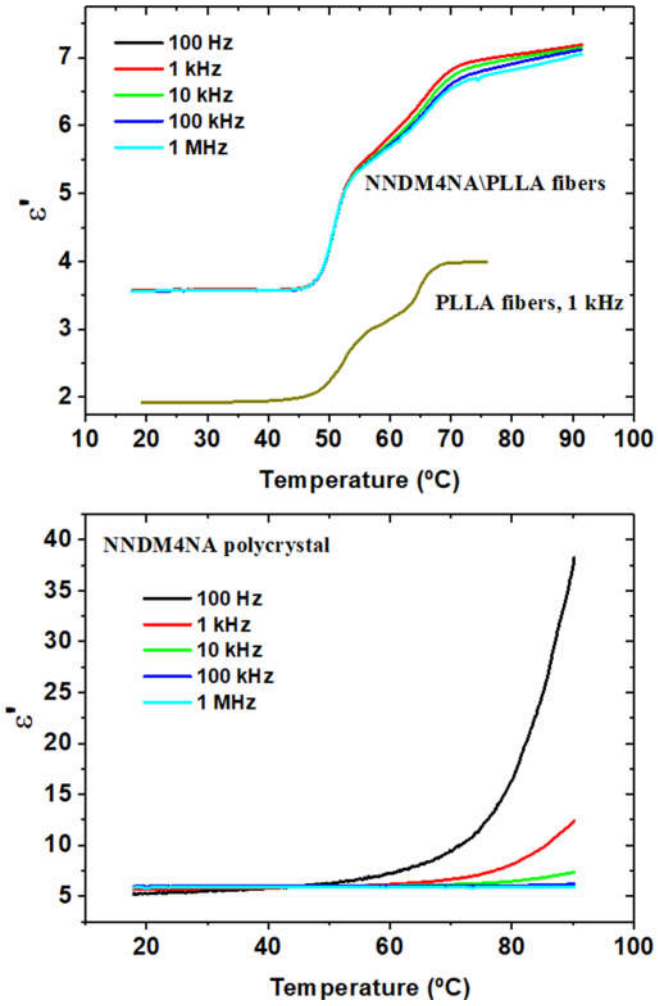

Figure 4. Temperature dependence of the dielectric constant (ε') at different frequencies of **(a)** NNDM4NA@PLLA and pure PLLA nanofiber array, **(b)** NNDM4NA polycrystalline pellet.

Pure PLLA polymer glass transition temperature was reported to occur in the range $T_{g,bulk}$ = 55-65ºC [49]. There is, for NNDM4NA@PLLA fibers, an increase the dielectric constant with temperature reaching 7 for frequencies between 100 Hz and 1MHz relatively to pure PLLA fibers. At room temperature and for all frequencies it is around 3.5 for NNDM4NA@PLLA fibers while for NNDM4NA pellet it is around 6, Figure 4 a) and b) respectively. NNDM4NA electrospun fibers have a dielectric constant significantly higher (approximately 75 %) than pure PLLA fibers, Figure 4 a), which results from the polycrystalline NNDM4NA contribution, confirming its successful incorporation inside the polymer matrix.

3.5. Nanofibers Piezoelectric Voltage

The piezoelectric effect is a phenomenon that arises when an applied uniform stress generates electric polarization inside a dielectric material, where an inter-conversion between mechanical and electrical stimulus is present. The requisite for a crystalline solid

Preprints (www.preprints.org) | NOT PEER-REVIEWED | Posted: 27 September 2022 doi:10.20944/preprints202209.0421.v1

to display the phenomenon is to have a crystal structure without inversion symmetry. NNDM4NA crystallizes in the polar point group 2, which is acentric. The tensor relationship between the polarization P_i and stress σ_j tensors is given by d_{ij}, the piezoelectric modulus according to the relation (written in the matrix notation) $P_i = d_{ij}\,\sigma_j$ [50]. Inside the electrospun fibers there is no preferential crystallographic orientation and the periodical forces were applied perpendicular to the fiber array and measured along the same direction, see Figure 5 c). There is therefore an overall polarization such that the piezoelectric modulus tensor is an effective coefficient, P (NNDM4NA@PLLA) = $d_{eff}\,\sigma$. The stress applied varied between 1.3×10^3 Nm^{-2} and 11.3×10^3 Nm^{-2}.

Extraordinarily, for NNDM4NA@PLLA fiber mats a 1.5 N applied periodical force originates respectively a 33 V and 330 nA maximum instantaneous output piezoelectric voltage and current, as shown in Figure 5 a). Here the two opposite peaks correspond respectively to the exerted and released force. A plot of the output voltage as a function of several applied periodical forces shows a linear increase of the response with the magnitude of the force as expected, Figure 5 b). We should note that there is a contribution from the PLLA polymer matrix of 100 nA, for the same applied force, as PLLA is itself a piezoelectric polymer. Under similar conditions, electrospun nanofiber mats fabricated with 3NA embedded into poly-ε-caprolactone (PCL) polymer, 3NA@PCL, originated an output voltage and current of 5 V and 50 nA, respectively [33]. Remarkably, NNDM4NA@PLLA output voltage is more than 6 times higher.

We can calculate the magnitude of d_{eff} from by integration of the induced piezoelectric current over a time period of 1 ms, $Q = \int I\,dt$. From our measurements, Figure 5 a), we obtained Q = 330 pC for NNDM4NA@PLLA fiber mats and Q = 220 pC considering only the contribution from NNDM4NA nanocrystals. The induced charge is related to the applied force by the equation $Q = d_{eff}\,F$. Therefore, an effective piezoelectric coefficient equal to d_{eff} = 220 pCN^{-1} for an NNDM4NA@PLLA fiber array and d_{eff} = 147 pCN^{-1} for nanocrystalline NNDM4NA, disregarding the polymer contribution. These values are extraordinarily high for an organic crystal which compare well with those of organic-inorganic ferroelectric perovskites trimethylchloromethyl ammonium trichloromanganese (TMCM)$MnCl_3$ and trimethylchloromethyl ammonium trichlorocadmium (TMCM)$CdCl_3$, respectively d_{33} = 230 pCN^{-1} and d_{33} = 185 pCN^{-1}, and barium titanate ($BaTiO_3$) with d_{33} = 190 pCN^{-1} [51-52].

Besides the piezoelectric coefficient magnitude, another relevant quantity is the piezoelectric voltage coefficient $g_{eff} = d_{eff}/(\varepsilon'\varepsilon_0)$ VmN^{-1}, which indicates the performance of a material as a piezoelectric generator. Crystals with high piezoelectric coefficients and low dielectric permittivity will originate high values of g_{eff}. For NNDM4NA@PLLA fibers, at room temperature ε' = 3.5 (Figure 5 a)), originating an effective piezoelectric voltage coefficient as high as g_{eff} = 7.1 VmN^{-1}. This value is one order of magnitude higher than that obtained for the 2-dimensional hybrid ferroelectric perovskite (4-aminotetrahydropyran)2 lead tetrabromide, $(ATHP)_2PbBr_4$, which exhibited an already large value of g_{eff} = 0.66 VmN^{-1} [53] twice of that displayed by a poly-vinylidene fluoride (PVDF) polymer thin film for which g_{eff} = 0.29 VmN^{-1} [54]. It is also interesting to compare the above values with those of biological dipeptides derivatives of diphenylalanine electrospun fibers embedded into PLLA, as indicated in Table 2.

Table 2. Piezoelectric output quantities for selected all organic electrospun nanofiber array.

Fiber array	Force/area [Nm^2]	V_{out} [V]	d_{eff} [pCN^{-1}]	g_{eff} [VmN^{-1}]	Ref.
NNDM4NA	$4x10^3$	33	147	7.1	This work
3NA	$4x10^3$	7	37	1.2	[33]
Boc-PhePhe	$4x10^3$	30	8.4	0.3	[31]
Boc-*p*NPhe*p*NPhe	$4x10^3$	58	16	0.6	[55]

Preprints (www.preprints.org) | NOT PEER-REVIEWED | Posted: 27 September 2022 doi:10.20944/preprints202209.0421.v1

The extraordinarily NNDM4NA nanocrystals piezoelectric response to an applied periodical stress results from its high molecular dipole moment, low crystallographic symmetry (point group 2), high tensile strength and Young modulus as well its low dielectric permittivity, combined with the piezoelectric properties of the PLLA polymer matrix. In this work we demonstrate that electrospun NNDM4NA@PLLA fibers are attractive composite nanomaterials as generators of high piezoelectric voltage as well blue luminescence.

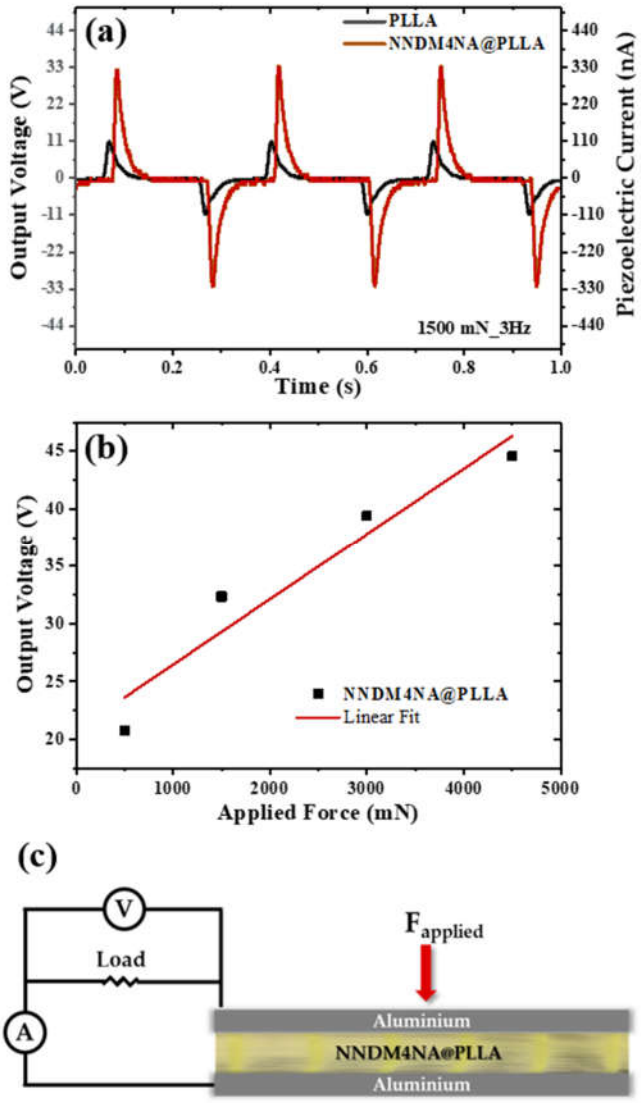

Figure 5. (a,b) Output voltage (V) and current (nA) measured through a load resistance of 100 MΩ on electrospun fiber array of PLLA and PLLA doped with NNDM4NA nanocrystals, **(c)** and schematic piezoelectric setup for NNDM4NA@PLLA fiber array.

4. Conclusions

Highly aligned poly-l-lactic acid polymer microfibers with embedded *N,N*-dimethyl-4-nitroaniline acentric nanocrystals, fabricated using the electrospinning nanofabrication technique were successfully produced containing the nanocrystals evenly spread in the fibers interior. The hybrid composite fibers displayed an extraordinarily high piezoelectric output response, where for a small stress of 5.0×10^3 Nm^{-2}, an effective piezoelectric voltage

coefficient of g_{eff} = 3.6 VmN^{-1} was obtained. This results from the low room temperature dielectric permittivity of 3.5 combined with one of the highest effective piezoelectric coefficients measured on organic crystals formed by electron donor-acceptor molecules (d_{eff} = 220 pCN^{-1}). The fibres were found to display solid state blue fluorescence with a long (147 ns) lifetime decay. Furthermore, the composite fibers exhibit an average increase of 67% on the Young modulus reaching 55 MPa, while the tensile strength reaches 2.8 MPa when compared with pure PLLA fibers. The results show that organic nanocrystals, from small organic molecules, with elastic and piezoelectric properties form hybrid functional 2-dimensional luminescent array which are mechanical strong and generate high output voltages making them promising for applications in energy harvesting and as solid-state blue emitters.

Supplementary Materials: The following supporting information can be downloaded at: www.mdpi.com/xxx/s1, Figure S1: title; Table S1: title; Video S1: title.

Author Contributions: Conceptualization, R.B. and E.G.; investigation, R.B., V.I., B.A., B.S., J.O., N.C., P.R., A.M., C.C., M.P. and M.B.; data curation, X.X.; writing—original draft preparation, R.B. and E.G.; writing—review and editing, R.B. and E.G.; supervision, R.B. and E.G.; project administration, R.B. and E.G.; funding acquisition, R.B. and E.G. All authors have read and agreed to the published version of the manuscript.

Institutional Review Board Statement: This study did not involve humans or animals.

Informed Consent Statement: This study did not involve humans or animals.

Acknowledgments: We acknowledge FEDER (European Fund for Regional Development)-COMPETE-QREN-EU for financial support through the Physics Centers of the Universities of Minho and Porto (Ref. UID/FIS/04650/2013 and UID/FIS/04650/2019). Part of this work was funded by national funds (OE), through FCT − Fundação para a Ciência e a Tecnologia, I.P., in the scope of the framework contract foreseen in the numbers 4, 5, and 6 of the article 23, of the Decree-Law 57/2016, of August 29, changed by Law 57/2017, of July 19.

Conflicts of Interest: The authors declare no conflict of interest.

References

1. Xu, J. L.; Semin, S.; Rasing, T.; Rowan, A. E. Organized chromophoric assemblies for nonlinear optical materials: towards (sub)wavelength scale architectures. *Small* **2015,** *11*, 1113-1129.
2. Bosshard, C.; Hulliger, J.; Florsheimer, M.; Gunter, P., *Organic nonlinear optical materials*. CRC press: 2001.
3. Garito, A.; Singer, K.; Teng, C. Molecular optics: nonlinear optical properties of organic and polymeric crystals. **1983**.
4. Nalwa, H. S.; Miyata, S., *Nonlinear optics of organic molecules and polymers*. CRC press: 1996.
5. Hashimoto, H.; Okada, Y.; Fujimura, H.; Morioka, M.; Sugihara, O.; Okamoto, N.; Matsushima, R. Second-harmonic generation from single crystals of n-substituted 4-nitroanilines. *Jpn. J. Appl. Phys.* **1997,** *36*, 6754-6760.
6. Trueblood, K. N.; Goldish, E.; Donohue, J. A three-dimensional refinement of the crystal structure of 4-nitroaniline. *Acta Crystallogr.* **1961,** *14*, 1009-1017.
7. Ayers, S.; Faktor, M. M.; Marr, D.; Stevenson, J. L. Growth of single crystals of meta-nitroaniline and the evaluation of its electro-optic properties. *J. Mater. Sci.* **1972,** *7*, 31-33.
8. Bain, A. M.; El-Korashy, N.; Gilmour, S.; Pethrick, R. A.; Sherwood, J. N. Ultrasonic and piezoelectric investigations on single crystals of 3-nitroaniline. *Philos. Mag. B* **1992,** *66*, 293-305.
9. Davis, D.; Sreekumar, K.; Sajeev, Y.; Pal, S. Optimization of nonlinear optical properties by substituent position, geometry and symmetry of the molecule: an ab initio study. *J. Phys. Chem. B* **2005,** *109*, 14093-14101.
10. Howard, S. T.; Hursthouse, M. B.; Lehmann, C. W.; Mallinson, P. R.; Frampton, C. S. Experimental and theoretical-study of the charge-density in 2-methyl-4-nitroaniline. *J. Chem. Phys.* **1992,** *97*, 5616-5630.
11. Paturle, A.; Graafsma, H.; Sheu, H. S.; Coppens, P.; Becker, P. Measurement of the piezoelectric tensor of an organic crystal by the x-ray method: The nonlinear optical crystal 2-methyl 4-nitroaniline. *Phys. Rev. B* **1991,** *43*, 14683-14691.
12. Levine, B. F.; Bethea, C. G.; Thurmond, C. D.; Lynch, R. T.; Bernstein, J. L. An organic crystal with an exceptionally large optical second-harmonic coefficient: 2-methyl-4-nitroaniline. *J. Appl. Phys.* **1979,** *50*, 2523-2527.
13. Oudar, J. L.; Le Person, H. Second-order polarizabilities of some aromatic molecules. *Opt. Commun.* **1975,** *15*, 258-262.
14. Frazier, C. C.; Cockerham, M. P.; Chauchard, E. A.; Lee, C. H. Second-harmonic generation in aromatic organic compounds. *J. Opt. Soc. Am. B* **1987,** *4*, 1899-1903.
15. Mak, T. C. W.; Trotter, J. The crystal and molecular structure of N,N-dimethyl-p-nitroaniline. *Acta Crystallogr.* **1965,** *18*, 68-74.

16. Borbulevych, O. Y.; Clark, R. D.; Romero, A.; Tan, L.; Antipin, M. Y.; Nesterov, V. N.; Cardelino, B. H.; Moore, C. E.; Sanghadasa, M.; Timofeeva, T. V. Experimental and theoretical study of the structure of N,N-dimethyl-4-nitroaniline derivatives as model compounds for non-linear optical organic materials. *J. Mol. Struct.* **2002,** *604*, 73-86.
17. Takamizawa, S.; Takasaki, Y.; Sasaki, T.; Ozaki, N. Superplasticity in an organic crystal. *Nat. Commun.* **2018,** *9*, 3984.
18. Edington, J. W.; Melton, K. N.; Cutler, C. P. Superplasticity. *Prog. Mater. Sci.* **1976,** *21*, 61-170.
19. Langdon, T. G. Grain boundary sliding revisited: Developments in sliding over four decades. *J. Mater. Sci.* **2006,** *41*, 597-609.
20. Krishna, G. R.; Devarapalli, R.; Lal, G.; Reddy, C. M. Mechanically flexible organic crystals achieved by introducing weak interactions in structure: supramolecular shape synthons. *J. Am. Chem. Soc.* **2016,** *138*, 13561-13567.
21. Gupta, P.; Allu, S.; Karothu, D. P.; Panda, T.; Nath, N. K. Organic molecular crystals with dual stress-induced mechanical response: elastic and plastic flexibility. *Cryst. Growth. Des.* **2021,** *21*, 1931-1938.
22. Saha, S.; Mishra, M. K.; Reddy, C. M.; Desiraju, G. R. From molecules to interactions to crystal engineering: mechanical properties of organic solids. *Accounts Chem. Res.* **2018,** *51*, 2957-2967.
23. Ghosh, S.; Mishra, M. K. Elastic molecular crystals: from serendipity to design to applications. *Cryst. Growth. Des.* **2021,** *21*, 2566-2580.
24. Greiner, A.; Wendorff, J. H. Electrospinning: a fascinating method for the preparation of ultrathin fibers. *Angew. Chem. Int. Ed.* **2007,** *46*, 5670-5703.
25. Reneker, D. H.; Yarin, A. L.; Fong, H.; Koombhongse, S. Bending instability of electrically charged liquid jets of polymer solutions in electrospinning. *J. Appl. Phys.* **2000,** *87*, 4531-4547.
26. Jana, S.; Cooper, A.; Ohuchi, F.; Zhang, M. Uniaxially aligned nanofibrous cylinders by electrospinning. *ACS Appl. Mater. Inter.* **2012,** *4*, 4817-4824.
27. Laramée, A. W.; Lanthier, C.; Pellerin, C. Electrospinning of highly crystalline polymers for strongly oriented fibers. *ACS Appl. Polym. Mater.* **2020,** *2*, 5025-5032.
28. Ding, J.; Zhang, J.; Li, J.; Li, D.; Xiao, C.; Xiao, H.; Yang, H.; Zhuang, X.; Chen, X. Electrospun polymer biomaterials. *Prog. Polym. Sci.* **2019,** *90*, 1-34.
29. Isakov, D. V.; de Matos Gomes, E.; Vieira, L. G.; Dekola, T.; Belsley, M. S.; Almeida, B. G. Oriented single-crystal-like molecular arrangement of optically nonlinear 2-methyl-4-nitroaniline in electrospun nanofibers. *ACS Nano* **2011,** *5*, 73-78.
30. Baptista, R. M. F.; Bernardo, C. R.; Belsley, M. S.; de Matos Gomes, E. Electrospun fibers with highly polarized second harmonic light from 2-amino-4-nitroaniline and 3-nitroaniline nanocrystals embedded in poly-L-lactic acid polymer. *Opt. Mater.* **2021,** *116*, 111089.
31. Baptista, R. M. F.; de Matos Gomes, E.; Raposo, M. M. M.; Costa, S. P. G.; Lopes, P. E.; Almeida, B.; Belsley, M. S. Self-assembly of dipeptide Boc-diphenylalanine nanotubes inside electrospun polymeric fibers with strong piezoelectric response. *Nanoscale Adv.* **2019,** *1*, 4339-4346.
32. Baptista, R. M. F.; Isakov, D.; Raposo, M. M. M.; Belsley, M.; Bdikin, I.; Kholkin, A. L.; Costa, S. P. G.; de Matos Gomes, E. Ferroelectric nanofibers with an embedded optically nonlinear benzothiazole derivative. *J. Nanopart. Res.* **2014,** *16*, 2502.
33. Bernardo, C. R.; Baptista, R. M. F.; de Matos Gomes, E.; Lopes, P. E.; Raposo, M. M. M.; Costa, S. P. G.; Belsley, M. S. Anisotropic PCL nanofibers embedded with nonlinear nanocrystals as strong generators of polarized second harmonic light and piezoelectric currents. *Nanoscale Adv.* **2020,** *2*, 1206-1213.
34. Papkov, D.; Delpouve, N.; Delbreilh, L.; Araujo, S.; Stockdale, T.; Mamedov, S.; Maleckis, K.; Zou, Y.; Andalib, M. N.; Dargent, E.; Dravid, V. P.; Holt, M. V.; Pellerin, C.; Dzenis, Y. A. Quantifying polymer chain orientation in strong and tough nanofibers with low crystallinity: toward next generation nanostructured superfibers. *ACS Nano* **2019,** *13*, 4893-4927.
35. Persano, L.; Camposeo, A.; Tekmen, C.; Pisignano, D. Industrial upscaling of electrospinning and applications of polymer nanofibers: A Review. *Macromol. Mater. Eng.* **2013,** *298*, 504-520.
36. Chang, J.; Dommer, M.; Chang, C.; Lin, L. Piezoelectric nanofibers for energy scavenging applications. *Nano Energy* **2012,** *1*, 356-371.
37. Kobayashi, J.; Asahi, T.; Ichiki, M.; Oikawa, A.; Suzuki, H.; Watanabe, T.; Fukada, E.; Shikinami, Y. Structural and optical properties of poly lactic acids. *J. Appl. Phys.* **1995,** *77*, 2957-2973.
38. Smith, M.; Calahorra, Y.; Jing, Q.; Kar-Narayan, S. Direct observation of shear piezoelectricity in poly-l-lactic acid nanowires. *APL Mater.* **2017,** *5*, 074105.
39. Kubelka, P. New contributions to the optics of intensely light-scattering materials. Part I. *J. Opt. Soc. Am.* **1948,** *38*, 448-457.
40. Raghavender, A. T.; Samantilleke, A. P.; Sa, P.; Almeida, B. G.; Vasilevskiy, M. I.; Hong, N. H. Simple way to make Anatase TiO_2 films on FTO glass for promising solar cells. *Mater. Lett.* **2012,** *69*, 59-62.
41. Kolev, T.; Koleva, B. B.; Spiteller, M.; Mayer-Figge, H.; Sheldrick, W. S. 2-Amino-4-nitroaniline, a known compound with unexpected properties. *J. Phys. Chem. A* **2007,** *111*, 10084-10089.
42. Khalil, O. S.; Seliskar, C. J.; McGlynn, S. P. Electronic spectroscopy of highly-polar aromatics.* II. Luminescence of nitroanilines. *J. Chem. Phys.* **1973,** *58*, 1607-1612.
43. Campoy-Quiles, M.; Ishii, Y.; Sakai, H.; Murata, H. Highly polarized luminescence from aligned conjugated polymer electrospun nanofibers. *Appl. Phys. Lett.* **2008,** *92*, 213305.

 doi:10.20944/preprints202209.0421.v1

44. Camposeo, A.; Persano, L.; Pisignano, D. Light-emitting electrospun nanofibers for nanophotonics and optoelectronics. *Macromol. Mater. Eng.* **2013,** *298*, 487-503.
45. Makuła, P.; Pacia, M.; Macyk, W. How to correctly determine the band gap energy of modified semiconductor photocatalysts based on UV–vis spectra. *J. Phys. Chem. Lett.* **2018,** *9*, 6814-6817.
46. Lee, D. W.; De Los Santos V, L.; Seo, J. W.; Felix, L. L.; Bustamante D, A.; Cole, J. M.; Barnes, C. H. W. The Structure of Graphite Oxide: Investigation of Its Surface Chemical Groups. *J. Phys. Chem. B* **2010,** *114*, 5723-5728.
47. Molares, M. E. T.; Buschmann, V.; Dobrev, D.; Neumann, R.; Scholz, R.; Schuchert, I. U.; Vetter, J. Single-crystalline copper nanowires produced by electrochemical deposition in polymeric ion track membranes. *Adv. Mater.* **2001,** *13*, 62-65.
48. Bognitzki, M.; Czado, W.; Frese, T.; Schaper, A.; Hellwig, M.; Steinhart, M.; Greiner, A.; Wendorff, J. H. Nanostructured Fibers via Electrospinning. *Adv. Mater.* **2001,** *13*, 70-72.
49. Farah, S.; Anderson, D. G.; Langer, R. Physical and mechanical properties of PLA, and their functions in widespread applications — A comprehensive review. *Adv. Drug Deliv. Rev.* **2016,** *107*, 367-392.
50. Nye, J. F., *Physical Properties of Crystals: Their Representation by Tensors and Matrices*. Oxford University Press: Oxford, 1985.
51. You, Y.-M.; Liao, W.-Q.; Zhao, D.; Ye, H.-Y.; Zhang, Y.; Zhou, Q.; Niu, X.; Wang, J.; Li, P.-F.; Fu, D.-W.; Wang, Z.; Gao, S.; Yang, K.; Liu, J.-M.; Li, J.; Yan, Y.; Xiong, R.-G. An organic-inorganic perovskite ferroelectric with large piezoelectric response. *Science* **2017,** *357*, 306.
52. Pan, Q.; Xiong, Y.-A.; Sha, T.-T.; You, Y.-M. Recent progress in the piezoelectricity of molecular ferroelectrics. *Mater. Chem. Front.* **2021,** *5*, 44-59.
53. Chen, X.-G.; Song, X.-J.; Zhang, Z.-X.; Li, P.-F.; Ge, J.-Z.; Tang, Y.-Y.; Gao, J.-X.; Zhang, W.-Y.; Fu, D.-W.; You, Y.-M.; Xiong, R.-G. Two-Dimensional Layered Perovskite Ferroelectric with Giant Piezoelectric Voltage Coefficient. *J. Am. Chem. Soc.* **2020,** *142*, 1077-1082.
54. Li, M.; Wondergem, H. J.; Spijkman, M.-J.; Asadi, K.; Katsouras, I.; Blom, P. W. M.; de Leeuw, D. M. Revisiting the δ-phase of poly(vinylidene fluoride) for solution-processed ferroelectric thin films. *Nat. Mater.* **2013,** *12*, 433-438.
55. Baptista, R. M. F.; Lopes, P. E.; Rodrigues, A. R. O.; Cerca, N.; Belsley, M. S.; de Matos Gomes, E. Self-assembly of Boc-p-nitro-l-phenylalanyl-p-nitro-l-phenylalanine and Boc-l-phenylalanyl-l-tyrosine in solution and into piezoelectric electrospun fibers. *Materials Adv.* **2022,** *3*, 2934-2944.